

# Multi-phase, non-isothermal transfer of water in a simple geometry

Pierre Lidon,<sup>1,2</sup> Etienne Perrot,<sup>1</sup> and Abraham D. Stroock<sup>1,3</sup>

<sup>1</sup>*Robert Frederick Smith School of Chemical and Biomolecular Engineering,  
Cornell University, 120 Olin Hall, Ithaca, NY, USA*

<sup>2</sup>*CNRS, Solway, LOF, UMR 5258, Univ. Bordeaux,  
178 avenue du Dr. Schweitzer, F-33600 Pessac, France\**

<sup>3</sup>*Kavli Institute at Cornell for Nanoscale Science, Physical Sciences Building, Ithaca, NY, USA<sup>†</sup>*

It has long been acknowledged that heat and water transport of in soils and plants are intimately coupled. Pioneering work by Philip and de Vries proposed the physical basis and governing equations to describe these processes; their theory has since been refined many times. However, the lack of appropriate sensors for in situ monitoring of water status has impeded clear interpretation of field experiments and no general consensus has emerged on a precise description of water transport in non-isothermal porous media. In this paper, we use a new microfluidic tool called the microtensiometer that measures water potential to study a simple model situation: we measure the evolution of water potential in a vapor gap across which a controlled temperature gradient is applied and report a decrease of water potential with temperature difference by  $-7.9 \pm 0.4 \text{ MPa.K}^{-1}$ , in agreement with previous experiments using other techniques. Based on a thermodynamic analysis of our system, we derive a theoretical prediction for this effect. Our model differs from Philip and de Vries equations by an additional water flux, negligible in our experiment but which should become significant in the case of unsaturated, nanoporous media. Both predictions by our model and by Philip and de Vries are close to the experimental value but with a discrepancy significant when compared with experimental uncertainties.

## INTRODUCTION

### Context

Recent estimates indicate that irrigated agriculture accounts for about 70 % of human water consumption and that crops exploit only 40 % of the water deployed [1]. In the current context of climate change and increasing food demand for a fast growing global population, limitations of water resources motivate the design of more sustainable agricultural practices with optimized irrigation processes. Such a goal requires the development of a precise and quantitative understanding of water fluxes across the soil-plant-atmosphere continuum (SPAC).

This question is an intrinsically multiscale, multiphase and multiphysics problem. In soils, liquid water frequently exists in a capillary condensed state, trapped inside the solid porous matrix and coexisting with an unsaturated vapor phase. Plants capture water via their roots and transport it towards the leaves where it evaporates into the atmosphere. Atmospheric conditions of humidity and temperature at the soil and canopy surface drives water fluxes and in turn, soil moisture exerts a feedback on the local climate [2, 3]. Water flow through the SPAC is thus a problem of coupled heat and mass transport in an heterogeneous porous environment and involving interactions between different scales, from microns for phenomena in soil pores and plant stomata to kilometers for the regional climate.

In their pioneering work, Philip and de Vries [4–7] (PdV) introduced a phenomenological model in the form of a set of coupled partial differential equations for the temperature and water saturation fields from a physical

description of transport processes in unsaturated porous media, as illustrated in Fig. 1. Their continuum theory accounts for gradients and fluxes averaged at mesoscale, i.e., on scales larger than the typical pore size [8–10]. This model was later reformulated by [11] to replace as an independent variable the water saturation by the water potential  $\Psi$  [Pa] introduced by [12], quantifying the distance to saturation of the water and defined by

$$\Psi(T, P) = \rho_\ell(\mu(T, P) - \mu_{\text{sat}}(T)). \quad (1)$$

where  $\mu(T, P)$  is the chemical potential of the water,  $\mu_{\text{sat}}(T) = \mu(T, P_{\text{sat}}(T))$  is the chemical potential at saturation and  $\rho_\ell [\text{m}^3]$  is the number density of the liquid phase. Finally, further improvements have been proposed to account for other microscopic phenomena and various imposed conditions encountered in experiments (e.g., the presence of solutes [13–15], convective flux induced by thermal dilation of the soil [16–18] of unsteady temperature conditions [19]). These models capture the essential physical phenomena at play in water transport in unsaturated and non isothermal porous media and can be, for instance, extended to describe transport in plants [20].

In the engineering litterature, PdV model and its variants were numerically analysed in multiple conditions (see e.g., [21–32]) in order to confront its predictions with results from laboratory (see e.g. [33–43]) or field experiments (see e.g. [19, 44–53]). Despite these numerous studies, no consensus has yet emerged in the soil hydrology community on the relevance of various ingredients of PdV model [16, 32, 54]. Several reasons explain this situation. First, realistic soils used in experiments

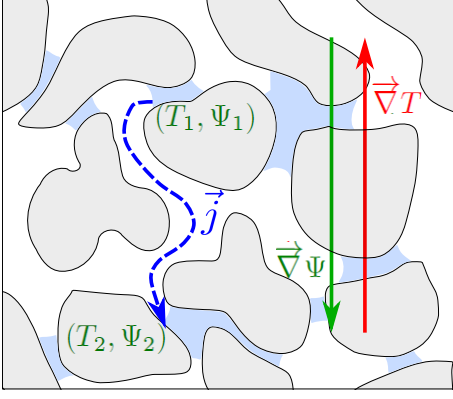


FIG. 1: Context of interest. Within the porous matrix, patches of capillary condensed liquid water coexist with a vapor phase in air. In the presence of a temperature gradient, a gradient of water potential is established which drives a net water flux,  $\vec{j}$  [ $\text{m}^{-2} \cdot \text{s}^{-1}$ ], through the medium. In PdV model, the gradient of water potential,  $\nabla \Psi$ , is proportional to the gradient of temperature,  $\nabla T$  (see Eq. (5)).

are complex systems, characterized by a large set of parameters and heterogeneity; it is hard to isolate specific causes for discrepancies between experimental measurements and numerical simulations and to obtain definitive conclusions on the validity of the model. Second, there is a lack of appropriate sensors to monitor soil status locally [55]. In particular, thermocouple-based psychrometers have been the most relevant tool available as they can provide appropriate sensitivity to water potential over a useful range [23]. Nonetheless, the use of psychrometers has been limited by challenges in their operation (e.g., due to microvolt-scale, transient signals) and in evaluating local temperature gradients with the air gap that must separate the sensing junction from the sample [56].

A few years ago, our group introduced a microfluidic device, called the microtensiometer that allows for the local (the sensor being smaller than  $\sim 1 \text{ cm}$ ) and continuous (with a response time  $\sim 1 \text{ min}$ ) measurement of water potentials down to  $\sim -20 \text{ MPa}$  [57]. Such a sensor, presented in Fig. 2, opens an opportunity to monitor water status within soils and plants and thus gives a new platform to explore PdV model. The microtensiometer complements the psychrometer in that it senses water potential by a distinct physical mechanism: tensiometry senses pressure (tension) in pure liquid water in equilibrium with the phase of interest; psychrometry measures the dewpoint temperature during a transient cooling cycle. The tensiometer also has potential advantages as practical technique for environmental measurements in the simplicity of the electronic signal (a direct current voltage across a resistor bridge) and capability to be placed in intimate thermal contact with the medium of interest.

In this paper, we take first step in this direction by considering a model situation in which we aim to isolate

precisely one of the terms of PdV model, corresponding to the coupling between water potential and temperature through an unsaturated vapor in a closed system at steady state. More precisely, as shown in Fig. 3(b), we measure the variations of water potential across a vapor gap with a controlled temperature gradient in a closed chamber containing a solution of known water potential at the bottom. It has been acknowledged that non-isothermal conditions induce a systematic bias on water potential measurement by psychrometers and we confirm here with a better accuracy the correction factor which has previously been proposed by [56] and [58], which respectively measure variations of  $-7.77 \text{ MPa} \cdot \text{K}^{-1}$  and between  $-7.53 \text{ MPa} \cdot \text{K}^{-1}$  and  $-7.84 \text{ MPa} \cdot \text{K}^{-1}$ . We then present a simple physical analysis, similar to that obtained by integrating PdV equations but which predicts the existence an additional flux. This flux is negligible in our situation but could induce noticeable deviations to PdV predictions for flows through nanoporous media. The predicted value is  $-8.4 \text{ MPa} \cdot \text{K}^{-1}$ , close to experimental values but with a discrepancy larger than the estimated uncertainty. This validates qualitatively the temperature-driven water flux introduced in PdV model but leaves the possibility for additional physical phenomena at play.

## MODELS

### Philip and de Vries model

In the formulation of PdV model by [11], the molecular flux of water per unit surface  $\vec{j}$  [ $\text{m}^{-2} \cdot \text{s}^{-1}$ ] is phenomenologically written as

$$\vec{j} = -k_\ell \vec{\nabla} \Psi + \rho_\ell k_\ell \vec{g} - \rho_\ell D_{T,a} \vec{\nabla} T - D \vec{\nabla} \rho \quad (2)$$

where  $k_\ell$  [ $\text{Pa}^{-1} \cdot \text{m}^{-1} \cdot \text{s}^{-1}$ ] is the permeability of the liquid path,  $\rho_\ell$  [ $\text{m}^{-3}$ ] is the molecular density of the liquid,  $\vec{g}$  [ $\text{m} \cdot \text{s}^{-2}$ ] is the gravity acceleration and  $D_{T,a}$  [ $\text{m}^2 \cdot \text{s}^{-1}$ ] is a surface diffusion coefficient. The first term correspond to a convective transport of liquid water, due to gradients of water potential and to gravitational force. The second term is associated with liquid diffusion at the surface of the grains driven by difference of surface tension induced by temperature gradient (Marangoni flow). Finally, the third term is associated with molecular diffusion in the vapor phase.

If equilibration between the liquid and gas phase at menisci is faster than the other time scales, the local equality of chemical potentials of water in both phase is governed by the Kelvin equation, which relates the density of vapor to temperature through:

$$\rho(T, \Psi) = \rho_{\text{sat}}(T) \exp\left(\frac{\Psi}{\rho_\ell k_B T}\right). \quad (3)$$

Putting Eq. (3) into Eq. (2), we see that the diffusive flux,  $-D\vec{\nabla}\rho$ , in the gas phase is the sum of one flux driven by the temperature gradient and another driven by the water potential gradient. A final ingredient in the PdV model is that the temperature gradient involved in the

vapor flux may be enhanced by a factor  $f$ , the necessity and physical origin of which are still subject to debate [16, 19, 24, 29, 32, 36, 44]. The total water flux in PdV model can thus be written as:

$$\vec{j} = - \left[ k_\ell + \frac{D\rho(T, \Psi)}{\rho_\ell k_B T} \right] \vec{\nabla}\Psi - \left[ \rho_\ell D_{T,a} + Df \left( \rho(T, \Psi) \frac{d \ln \rho_{\text{sat}}}{dT} - \frac{\rho(T, \Psi)\Psi}{k_B T^2 \rho_\ell} \right) \right] \vec{\nabla}T + \rho_\ell k_\ell \vec{g}. \quad (4)$$

If the flux driven by gravity is negligible, for a closed system where  $\vec{j} = \vec{0}$ , we obtain that the gradients of water potential and of temperature are proportional according to:

$$\vec{\nabla}\Psi = - \frac{\rho_\ell D_{T,a} - \frac{Df\rho}{T} \left( \frac{\Psi}{\rho_\ell k_B T} - \frac{T}{P_{\text{sat}}} \frac{dP_{\text{sat}}}{dT} \right)}{k_\ell + \frac{D\rho}{\rho_\ell k_B T}} \vec{\nabla}T. \quad (5)$$

In our experiment, we will not consider any surface diffusion so that  $D_{T,a} = 0$ , there will be no direct liquid path so that  $k_\ell = 0$ . In order to keep the analysis minimal, we will not consider any enhancement factor and set  $f = 1$ . Under these hypotheses relevant to our situation, Eq. (5) reduces to:

$$\vec{\nabla}\Psi = \rho_\ell k_B \left( \frac{\Psi}{\rho_\ell k_B T} - \frac{T}{P_{\text{sat}}} \frac{dP_{\text{sat}}}{dT} \right) \vec{\nabla}T. \quad (6)$$

### Physical analysis of the experimental system under study

Our experimental system is far simpler than the situation considered in PdV model. We now propose a simple physical analysis of the phenomena at play when only a vapor path connects two points along a temperature gradient, as in our experiment (see Fig. 3). We will find a very similar result to that of the PdV model except for the prediction of an additional flux. We consider a closed porous medium filled with water vapor and air, with a permeability  $k_v [\text{Pa}^{-1} \cdot \text{m}^{-1} \cdot \text{s}^{-1}]$  for vapor in the gas path. In our experiments, this gas-filled medium is composed of a macroscopic tube closed at its sides by porous separators (see Fig. 3).

When a temperature difference is imposed between the two ends of the tube, dilation of the gas generates a density gradient in the medium which in turn creates a diffusive flux,  $-D\nabla\rho$ , described by Fick's law. This flux is accompanied by the formation of a pressure gradient, which, in turn, induces a backward convective flux,  $-k_v \nabla P$ , described by Darcy's law. This pressure gradient is not accounted for in the typical PdV treatment.

The total molecular water flux per unit surface in the medium,  $\vec{j} [\text{m}^{-2} \cdot \text{s}^{-1}]$ , is thus given by:

$$\vec{j} = -D\vec{\nabla}\rho - k_v \vec{\nabla}P \quad (7)$$

where  $D [\text{m}^2 \cdot \text{s}^{-1}]$  is the diffusion coefficient of the water molecules,  $\rho [\text{m}^{-3}]$  the molecular density of the gas phase and  $P [\text{Pa}]$  is the vapor pressure.

As the system is closed, there is no net water flux such that  $\vec{j} = \vec{0}$ : the diffusive flux generated by the thermal dilation of the gas is exactly compensated by the convective flux generated by the induced pressure gradient. If we assume the vapor is ideal, the equation of state,  $P = \rho k_B T$ , allows us to establish a direct link between the pressure and temperature gradients, based on Eq. (7):

$$\vec{\nabla}P = \frac{P}{T} \frac{1}{1 + k_v k_B T / D} \vec{\nabla}T. \quad (8)$$

Eq. (8) shows that the convective flux in Eq. (7) is proportional to the gradient of temperature: this relation should not be confused with Soret effect. Soret effect indeed deals with another phenomenon corresponding to differential migration of species of a mixture in a temperature gradient. It was initially observed in salt solution [59] and later gaseous and liquid mixtures [60]. In gas mixtures, it can be predicted from kinetic theory [61], while, in liquids, its explanation remains elusive [62]. In a mixture of water vapor and other gases, Soret effect may play a role but is unlikely to be significant near ambient temperature and humidity because the mole fraction of water in the gas is small [61].

At equilibrium, the chemical potential is the same in the liquid and vapor phases so, by assuming that the vapor is ideal, we have:

$$\mu(T, P) = \mu_{\text{sat}}(T) + k_B T \ln \left( \frac{P}{P_{\text{sat}}(T)} \right) \quad (9)$$

where  $P_{\text{sat}}(T)$  is the vapor saturation pressure and  $P/P_{\text{sat}}$  is the relative humidity of the vapor. We can use the water potential,  $\Psi$ , defined by Eq. (1) instead of

the chemical potential as a variable. By computing the gradients of Eq. (1) and Eq. (9), we obtain:

$$\vec{\nabla}\Psi = \rho_\ell k_B \left( \frac{\Psi}{\rho_\ell k_B T} - \frac{T}{P_{\text{sat}}} \frac{dP_{\text{sat}}}{dT} + \frac{1}{1 + k_v k_B T/D} \right) \vec{\nabla}T. \quad (10)$$

The first term in Eq. (10) stems from the direct dependency of  $\Psi$  in temperature and is negligible for water potentials of magnitude smaller than  $\rho_\ell k_B T \sim 120$  MPa near ambient; our experiments do not approach this limit, but it could occur within soils or other porous media. The second term in Eq. (10) comes from the variations of saturation pressure with temperature: this term should typically be dominant. By using tabulated data from [63], evaluation of this second term at the temperature of our experiment  $T = 21^\circ\text{C}$  gives:

$$\left. \frac{d\Psi}{dT} \right|_{\text{th}} = -8.47 \text{ MPa} \cdot \text{K}^{-1}. \quad (11)$$

The third term in Eq. (10) is related to the pressure gradient that arises to counterbalance the diffusive flux. It is possible to get a deeper insight in this effect by taking explicit expressions for the various coefficients as a function of molecular properties. For a porous medium, a typical form of the permeability is  $k_v = a\rho r^2/\eta$ , where  $a$  is a dimensionless prefactor and depends on the topology of the medium and  $r$  is the typical pore size of the medium (average pore radius in a porous medium or radius of the glass tube in our experiment) [64]. Kinetic theory of perfect gases leads to a relationship  $\eta D = b k_B T / \rho \sigma^4$  between the viscosity and the diffusion coefficient, where  $b$  is a dimensionless factor depending on the shape of the molecule and  $\sigma[\text{m}]$  is a molecular diameter. Therefore we can rewrite the ratio that appears in Eq. (10) as:

$$\frac{k_v k_B T}{D} \sim (\rho \sigma^2)^2 r^2 = \left( \frac{r}{\ell} \right)^2 \quad (12)$$

where  $\ell = 1/\sqrt{\rho\sigma}$  is the mean free path of a gas molecule. Consequently, the pressure gradient becomes significant only for pores smaller than the mean free path, i.e., in the rarefied gas or Knudsen regime. At ambient pressure,  $\ell \sim 0.1 \mu\text{m}$  so this last term is generally negligible in granular materials. However, it could induce noticeable corrections for the transport in nanoporous materials such as clays.

The experimental situation we consider (see Fig. 3) can also be studied in the framework of the PdV model: then, there is no liquid path connecting the reservoir to the tensiometer so  $k_\ell = 0$  and there is no porous medium so  $D_{T,a} = 0$  and  $f = 1$ . In this case, Eq. (5) for the full PdV model reduces to Eq. (6) which is very similar to our Eq. (10). The only difference resides in the effect of the pressure gradient in the gas phase, that we have seen to be negligible in usual conditions and in the experiments reported here. It is to be noted that considering

a convective transport in the vapor phase was proposed by [17, 18] to model the effect of an airflow within the porous medium generated by the thermal dilation of the soil; that case is thus a different phenomenon than the one we consider here.

## MATERIALS AND METHODS

### Microtensiometer

In this sub-section, we only recall the working principles of the microtensiometer; further details on the fabrication has been published elsewhere [57]. The microtensiometer is a microfluidic tool designed to measure water potential in unsaturated phases. The size of the chip is of five millimeters on a side; when packaged, the size of the sensor is of order of centimeter. This small size allows for local measurement. Relative to the design presented by [57] improvements on the design of the chip allowed reduced response times down to a few minutes, such that it can capture typical dynamics of water potential across the SPAC.

Fig. 2 presents pictures of the microtensiometers used in this study. The key elements of this design are:

1. An internal cavity ( $1 \text{ mm} \times 2.5 \text{ mm} \times 3 \mu\text{m}$ ) formed by dry etching in a single crystal silicon wafer  $\langle 111 \rangle$  and filled with liquid water in a pressure chamber ( $\sim 3.5 \text{ MPa}$  during  $\sim 10 \text{ h}$ ) before use.
2. A strain gauge formed of a piezoresistive polysilicon on the opposite side of the silicon wafer from the cavity. The piezoresistors form a Wheatstone bridge.
3. A platinum resistance thermometer (PRT) on the top side of the silicon.
4. A layer of porous silicon ( $5 \mu\text{m}$ -thick) formed by anodization on the side of the wafer that contains the cavity. This layer provides a connected path of nanoscopic (average pore radius  $r_p \simeq 1.7 \text{ nm}$ ) from the cavity to one edge of the device. We have characterized the hydraulic and wetting properties of this material previously [65].
5. Microfluidic veins that partially span the distance between the cavity and the edge within porosified region. These veins increase the permeability of the path between the cavity and the edge.
6. A glass wafer anodically bonded to the side of the wafer with the cavity and veins.

Under isothermal conditions, corresponding to  $T_1 = T_2$  in the scenario detailed in Fig.3(b)), both thermal and mass transfer equilibria are reached: the temperature of

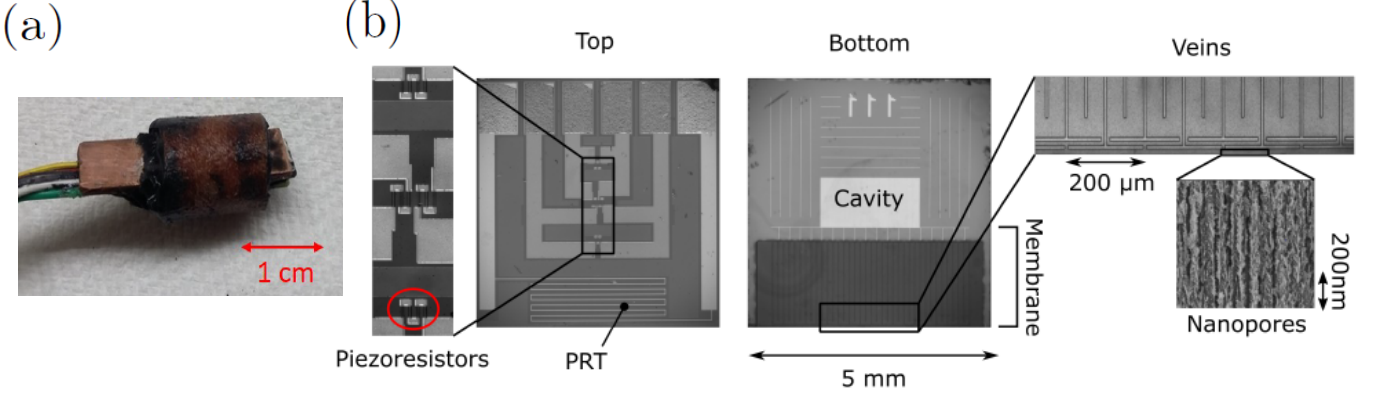


FIG. 2: Pictures of the tensiometer. (a) Global view of a packaged tensiometer with a copper strip. See Fig. 3(a,b) for a schematic diagram of the packaged device. (b) Details of the tensiometer. The top view shows the piezoresistors (an example circled in red) that constitute the strain gauge to measure deformations of the diaphragm and the platinum wire used as PRT. The bottom view shows the cavity containing bulk water and the nanoporous membrane (dark on the picture) connecting it with the outside. Microfluidic veins are etched in the membrane without linking directly the cavity and the outside in order to decrease response time of the device. Image credit (b): Antoine Robin.

the pure liquid in the cavity,  $T_1$ , equals that of the reference solution,  $T_2$ , and the water potentials of the internal liquid,  $\Psi_1$ , the vapor phase,  $\Psi_{\text{vap}}$ , and the reference solution,  $\Psi_2$ , are equal. Given that the water potential of the bulk, pure liquid water is just its difference in pressure from the standard state  $\Psi_1 = P_\ell - P_0$  and the water potential of the vapor is given by Eqs. (1) and (9), we have:

$$\Psi_1 = P_\ell - P_0 = \rho_\ell k_B T \ln \left( \frac{P}{P_{\text{sat}}(T)} \right) = \Psi_{\text{vap}} = \Psi_2, \quad (13)$$

where  $P_\ell$  is the pressure and  $\rho_\ell$  the number density of the liquid phase. This equilibrium is allowed by the curvature of the liquid/gas menisci at the mouth of the nanopores in the membrane; this curvature causes a reduction of the pressure of the liquid in the cavity, as shown in Fig. 3(c).

The internal cavity was closed by a diaphragm of plain silicon; the pressure difference between the liquid in the cavity and the external atmosphere deforms this diaphragm. This deformation was measured with a strain gauge made of a Wheatstone bridge of piezoresistors deposited on the diaphragm; after a preliminary calibration, it was possible to obtain water potential from the voltage across the bridge.

We calibrated the response of the strain gauge in two ways: first, we measured the voltage across the Wheatstone bridge (with fixed applied voltage 0.4 V) as a function of mechanically applied differences of pressure; second, we measured voltage as a function of water potential in an external vapor under isothermal conditions. According to Eq. (13), these two methods should provide the same result. As we discuss in section , we observed a systematic difference between the calibrations ( $\Delta V$  vs.  $\Delta P$  and  $\Delta V$  vs.  $\Psi$ ). Here, we describe the mechanical calibration; in section , we describe the osmotic one.

The microtensiometer was calibrated mechanically with the cavity filled with air and porous membrane sealed with latex paste (Liquid Latex Fashions). We then put the device in a pressure bomb (High Pressure Equipment Company; Erie, PA) in which we increased the pressure stepwise by injecting pressurized gas; the pressure outside the tensiometer thus increase while the pressure inside the cavity remained constant (note that appropriate safety precautions should be taken when working with fluids at elevated pressures). Consequently the diaphragm was pushed into the cavity; this mechanical deformation mimicked what happens with a filled tensiometer in presence of an unsaturated atmosphere such that the inner pressure decreased. For each step, after equilibration, we measured the voltage of the Wheatstone bridge; the observed response increased linearly with the pressure difference with an offset.

The microtensiometer is equipped with a thermometer made of a thin-film platinum wire deposited on the backside of the wafer, over the porous membrane. This wire serves as a platinum resistance thermometer (PRT): the resistance of the wire increased linearly with temperature. We calibrated the PRT in temperature against a commercial PRT (Omega) by placing them together in a water bath and changing its temperature stepwise. In this situation, the cavity and membranes were filled with liquid water and the voltage from the Wheatstone bridge was equal to its offset  $\Delta V_0$ , corresponding to saturated conditions. We observe that  $\Delta V_0$  depended slightly on temperature; this effect induced a small systematic uncertainty which is negligible as compared to other sources of uncertainty discussed in a later section.

## Experimental setup

The setup is depicted on Fig. 3. The microtensiometer was glued to a copper strip on its glass slide. We placed the system in a plastic tube which was filled with a curable urethane resin (UR5041, Electrolube) such that at one end the nanoporous membrane slightly emerged from the tube. In this package, the diaphragm of the tensiometer was protected from the resin and so that in the final device, it was covered by small air pocket, in order to avoid deformations of the diaphragm due to thermal expansion of the urethane. We capped the end of the device with a glass tube closed at the other extremity by a hydrophobic mesh (Mo-Flow Ventilation, mesh size  $\sim 0.5$  mm) and dipped it in a solution of known water potential. This hydrophobic mesh allowed for exchange of vapor but excluded the entry of liquid. The liquid water in the microtensiometer thus equilibrated with the solution through the vapor in the tube. This gas-filled tube volume mimics a pore in the classic PdV scenario (Fig. 1).

We placed the reference solution whose temperature was controlled by a water bath. We measured the temperature of the solution with a commercial PRT placed as closely as possible to the hydrophobic mesh. The bath was closed by a plate of insulating foam in which we drilled a tight hole to insert the tensiometer with the copper strip protruding. A Peltier module (Digikey Electronics, 1681-1028-ND) attached to the exposed end of the copper strip, controlled the temperature of the tensiometer.

A datalogger (CR6, Campbell Research Scientific) acquired data from the tensiometer and the commercial PRT in the solution. It then delivered a voltage proportional to the difference,  $\Delta T$ , between the temperature of the tensiometer and that of the solution to an Arduino board. A PID controller programmed on the Arduino switched the power supply of the Peltier module in order to impose a target temperature difference between the tensiometer and the reference solution. At steady state, this feedback loop provided a temperature difference with fluctuations of order  $0.05^\circ\text{C}$ . This fluctuation constituted a random source of uncertainty on the temperature difference that was smaller than the systematic uncertainty from the PRT calibrations. Another source of systematic uncertainty came from the intrinsic problem of thermometry: a thermometer measures its own temperature that may not be fully equilibrated with the temperature of the studied object. Thus, the temperature difference  $\Delta T^*$  measured by our device could be different from the temperature difference of interest,  $\Delta T$ , as will be discussed later.

Finally, this whole setup allowed us to measure the change in water potential of the liquid water in the cavity of the tensiometer for different values of the temperature

difference across the vapor gap in the glass tube. In the following, we consider experiments during which we imposed steps of measured temperature difference,  $\Delta T^*$ , by keeping the solution at constant temperature and modifying the temperature of the tensiometer with Peltier module. We monitored the evolution of water potential continuously. In general, steps of  $\sim 20$  min were long enough to allow for equilibration of the device.

## RESULTS

### Experiments in water

First, we used deionized water as the reference solution. By definition (Eq. (13)), its water potential is zero at any temperature and atmospheric pressure and the variations of water potential measured by the tensiometer reflect the changes of RH in the vapor at the interface of the nanoporous membrane. The result is displayed on Fig. 4.

As seen in Fig. 4, the obtained variations of  $\Psi$  with the measured difference of temperature,  $\Delta T^*$ , can be divided into two parts. At larger negative values of  $\Delta T^*$ , measured water potential was zero. While we may expect a positive water potential in this case, it is not possible to measure positive water potentials with our device: as the nanoporous membrane is hydrophilic, when the tensiometer is colder than the solution, water condenses and spreads on it so that no pressure difference can be maintained between the liquid in the cavity and the extended environment. At positive  $\Delta T^*$ , we observe a linear decrease of water potential with the difference of temperature.

We note, though, that the measured water potential vanishes for  $\Delta T^* \neq 0$ ; this observation illustrates the aforementioned problem with temperature measurement. First, due to finite thermal conductivity of water and porous silicon, we cannot rule out the existence of temperature gradients between the on-chip PRT and the cavity in the tensiometer, and between the reference PRT and the liquid-vapor interface in the solution. These discrepancies would cause a linear relationship  $\Delta T^* = \gamma \Delta T$  with  $\gamma \neq 1$ . Moreover, heat conduction can occur between the external atmosphere and the solution through the metallic wires of the PRT and through the glass tube which is not perfectly insulated. This leakage would create an offset between  $\Delta T^*$  and  $\Delta T$ . Thus, in general, we expect the following relationship between the actual and observed temperature difference:  $\Delta T^* = \gamma \Delta T + \theta$ .

Given that water potential vanishes for  $\Delta T^* \neq 0$  we conclude that an offset,  $\theta = \Delta T - \Delta T^*$ , exists; we determined this offset, with a good precision, by taking the intersection between the abscissa axis,  $\Psi = 0$ , and a linear fit over the points of non-zero water potential in plots as in Fig. 4. In order to get a good estimate of

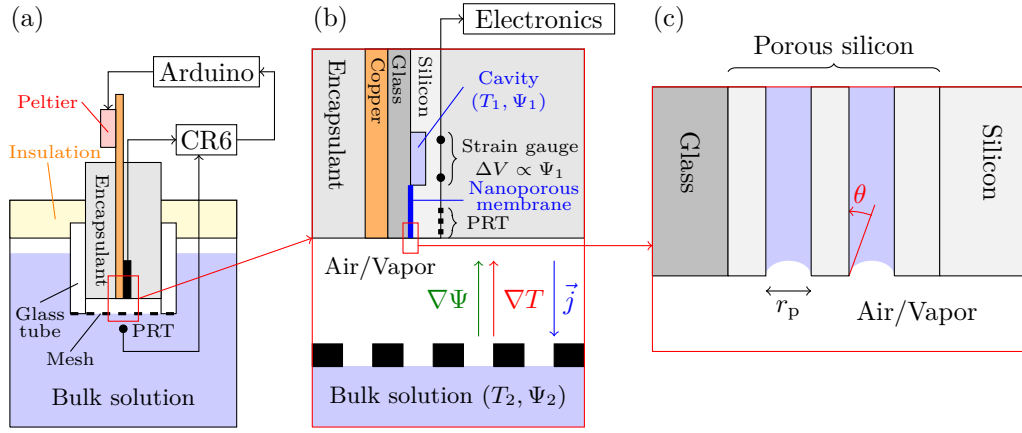


FIG. 3: Schematic diagrams of the experimental setup (not on scale). (a) Cross-sectional view of the experimental setup. The tensiometer (in black) is glued to a copper strip (in orange) and packaged in urethane (in gray). The device is capped by a glass tube (in white) closed by a porous hydrophobic mesh (dashed line) and dipped in an osmotic solution of known water potential (in blue) through a thermal insulation (in light yellow). Temperature of the tensiometer is controlled by a Peltier module (in pink) attached at the emerging end of the copper strip and powered through an Arduino-based feedback loop imposing a constant temperature difference with the solution. (b) Expanded view of the vapor gap. While the temperature of the solution,  $T_2$ , is imposed by a thermostat, that of the tensiometer,  $T_1$ , is controlled with a Peltier element connected to the copper strip on which the tensiometer is glued with thermal paste. When a temperature difference is imposed, there is a difference between the water potential measured by the tensiometer,  $\Psi_1$ , and that of the solution,  $\Psi_2$ . The water potential in the cavity is obtained by measuring the deformation of the diaphragm with the strain gauge, giving a voltage  $\Delta V$  proportional to  $\Psi_1$ . (c) Expanded view of the nanoporous membrane. When in contact with an unsaturated vapor, curvature of the menisci at the pore mouth decreases the pressure of the pore liquid to achieve mechanical equilibrium.

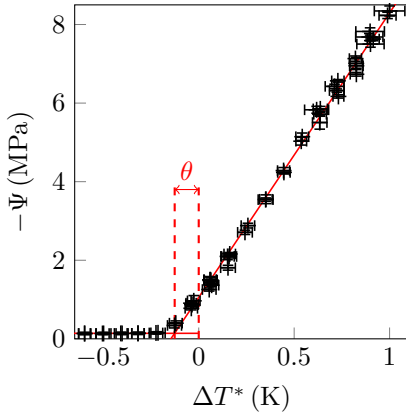


FIG. 4: Evolution of the water potential  $\Psi$  measured by the tensiometer ( $\Psi_1$  in Fig.3(b)) with the measured difference of temperature,  $\Delta T^*$ , between the tensiometer and pure liquid water. The red lines are linear regressions to determine the offset between the measured difference,  $\Delta T^*$ , and the true difference,  $\Delta T = \Delta T^* + \theta$ .

the slope  $d\Psi/dT$ , it is crucial to measure correctly the temperature difference between the water in the cavity of the tensiometer and the reference solution and thus to evaluate the factor  $\gamma$ . Because the thermal conductivity of porous silicon and water are large relative to air, we expect that the temperature of the PRT in the tensiometer is the same as this of the water in the cavity and that the temperature in the solution is homogeneous. We

confirmed this hypothesis by a further experiment: we removed the hydrophobic mesh and placed the tip of the commercial PRT entered slightly inside the vapor gap. In this geometry, the temperature offset was eliminated ( $\theta = 0$ ) but the observed slope did not change. Consequently, we consider that  $\gamma = 1$ . In what follows, we correct the measured temperature difference  $\Delta T^*$  by the offset,  $\theta$ , as determined in Fig. 4 to obtain the temperature difference between the solution and the tensiometer,  $\Delta T$ . The principal source of uncertainty in  $\Delta T$  comes from our estimation of  $\theta$ . Given the dependence of  $\theta$  on the precise position of the PRT, we evaluated  $\theta$  in each experiment, as shown in Fig. 4.

### Experiments in osmotic solutions

We repeated this experiment with different solutions of solutes (sodium chloride, urea, PEG) in order to have reference solutions of varying water potentials. The reference water potential,  $\Psi_{\text{ref}}$ , of these solutions was determined by using a chilled mirror hygrometer (WP4C, Meter Group). As we worked in dilute solutions, water potential of the solution did not vary strongly with temperature and in most experiments the temperature of the water bath was kept at its ambient value, at which the measurement of reference potential was performed.

For each reference  $\Psi$  as a function of  $\Delta T^*$  and assessed  $\theta$ , as illustrated in Fig. 4. Results (Fig. 5)



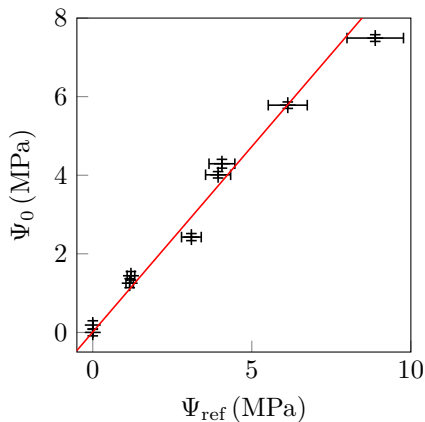


FIG. 5: Water potential for isothermal conditions,  $\Psi_0$ , measured by the tensiometer as a function of the water potential of the solution,  $\Psi_{\text{ref}}$ , determined by a chilled mirror hygrometer.

were very similar to what we observed with water (Fig. 4), except that the measured water potential in isothermal conditions  $\Psi_0 = \Psi(\Delta T = 0)$  was non-zero. This shift allowed for the measurement of water potentials for  $\Delta T < 0$ , as long as  $\Psi < 0$ .

First, we can compare the water potential  $\Psi_0$  with the reference value  $\Psi_{\text{ref}}$  obtained from the hygrometer, as presented on Fig. 5. We observe a linear relationship

$$\Psi_0 = \alpha \Psi_{\text{ref}} + \beta \quad (14)$$

where  $\alpha = 0.94 \pm 0.05$  and  $\beta = 0.10 \pm 0.06$  MPa.

As the mechanical calibration described in paragraph is supposed to mimic the behaviour of the system in presence of an unsaturated atmosphere, we expect  $\alpha = 1$  and  $\beta = 0$  MPa, but we observed a small discrepancy. With this data, we performed a so called osmotic calibration by comparing the measured voltage from the Wheatstone bridge with a reference water potential. This protocol is longer and more complex to perform, as it requires careful establishment of isothermal conditions, and gives a poorer precision than the mechanical calibration, but it is directly based on the phenomenon exploited by the microtensiometer (i.e. equilibrium with an unsaturated vapor). Thus, for all further analysis, we corrected the measured water potential by this factor  $\alpha$ , in order to eliminate any possible systematic uncertainty coming from a difference of behavior between the mechanical and osmotic protocols.

Finally, for every solution, we plotted the difference between the reference water potential measured in isothermal conditions and the water potential under an imposed temperature gradient,  $\Psi_0 - \Psi$ . This subtraction allows us to eliminate the offset due to the reference potential. The resulting aggregation of data is plotted on Fig. 6.

We observe that, independently of the reference value of water potential and of the nature of the reference so-

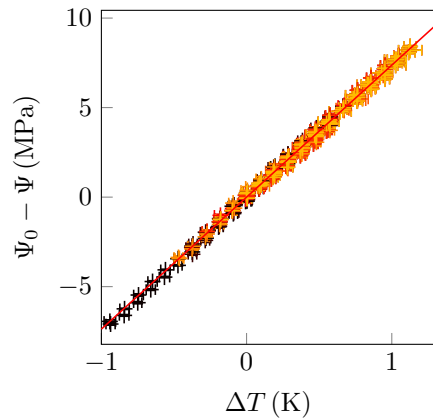


FIG. 6: Variation of water potential measured by the tensiometer relative to the value in isothermal conditions,  $\Psi_0 - \Psi$ , for several solutions of different  $\Psi_0$  (pure water  $\Psi_0 = 0$  MPa; urea solutions  $\Psi_0 = 1.16, 3.10, 3.94, 4.06, 6.13$  and  $8.88$  MPa; PEG solution  $\Psi_0 = 1.2$  MPa). Lighter colors correspond to increasing absolute water potential  $|\Psi_0|$ . The red line is a linear fit.

lution, water potential decreased linearly with the temperature difference with a constant slope

$$\left. \frac{d\Psi}{dT} \right|_{\text{exp}} = -7.9 \pm 0.4 \text{ MPa} \cdot \text{K}^{-1}. \quad (15)$$

We performed all experiments shown in Fig. 6 at the same bath temperature,  $T_{\text{bath}} = 21^\circ\text{C}$ . We however reproduced the experiment for different bath temperatures between  $T_{\text{bath}} = 15^\circ\text{C}$  to  $T_{\text{bath}} = 30^\circ\text{C}$  (data not shown): we observed a trend of a decreasing (absolute) slope with increasing temperature but within the error-bars. This trend is consistent with our theory (Eq. (10)) that predicts a range of slope from  $-8.71 \text{ MPa} \cdot \text{K}^{-1}$  to  $-8.12 \text{ MPa} \cdot \text{K}^{-1}$  between  $15^\circ\text{C}$  and  $30^\circ\text{C}$ .

Finally, it is noteworthy to comment on the discrepancies between the mechanical and osmotic calibrations. The existence of a different offset for both calibrations is not surprising: the mechanical calibration is performed on a microtensiometer before packaging it in urethane. Even if the diaphragm is protected during the process, packaging could exert stresses on the chip and thus induce a residual deformation of the strain gauge. Regardless, as we are only interested in water potential variations in this experiment, this offset has no impact on our results (Eq. (15)). The parameter  $\alpha$  is not far from its expected value ( $\alpha = 1$ ) but there is a slight deviation, corresponding to an overestimation of water potential with the mechanical calibration. This discrepancy could be due to a difference of the deformation resulting from an increase of pressure in the surrounding atmosphere and of a decrease of pressure in the cavity. Another, more likely, possibility is that the mechanical calibration has been limited up to pressures of  $6.0$  MPa while we are



measuring water potentials on a larger range down to  $\sim -10$  MPa here, which could have an impact on the results of fitting procedures. For these reasons, we believe the osmotic calibration is more reliable.

## DISCUSSION

As mentioned earlier, [56] previously studied the coupling between water potential and temperature gradient for temperature correction of thermocouple psychrometers. The authors propose a model similar to ours (at least outside of the Knudsen regime) and report a measured variation of  $-7.77 \text{ MPa} \cdot \text{K}^{-1}$  at  $T = 25^\circ\text{C}$ . In a more precise study by [58], they obtain a value between  $-7.53 \text{ MPa} \cdot \text{K}^{-1}$  and  $-7.84 \text{ MPa} \cdot \text{K}^{-1}$ . The authors did not report uncertainty.

These previously reported values agree quantitatively with our result (Eq. (15)) if we account for our uncertainty. Our study confirms this value with a more careful estimation of experimental uncertainties. We also explored a larger range of temperature difference (up to 2 K) for both positive and negative differences in various solutions. The previous studies were restricted to positive temperature differences below 0.1 K in water.

The variation of water potential we measured are inconsistent with our theoretical prediction ( $-7.9 \pm 0.4 \text{ MPa} \cdot \text{K}^{-1}$  in experiment vs.  $-8.47 \text{ MPa} \cdot \text{K}^{-1}$ ), despite the discrepancy being moderate. In our experiment, we cannot exclude a residual systematic uncertainty on the measurement of temperature difference between both sides of the vapor gap. However, when considering their positions in the setup, it is more likely that our measurement underestimates the true temperature gradient, which would imply that the coupling between water potential and temperature is smaller than our estimate. This is further supported by another test: as mentioned in , we repeated the experiment by placing the tip of the reference PRT inside the vapor gap. In this situation, there was no offset in the difference of temperature, i.e., the water potential measured by the tensiometer vanished when the measured difference of temperature was zero ( $\theta = 0$  in Fig. 4) and we obtained exactly the same value for the slope  $d\Psi/dT$ , i.e.,  $-7.9 \text{ MPa} \cdot \text{K}^{-1}$ . Another possible mistake in our analysis is the use of the osmotic calibration. If we keep the results provided by the mechanical one, the value we obtain is smaller  $(d\Psi/dT)_{\text{exp, mech}} = -7.45 \pm 0.2 \text{ MPa} \cdot \text{K}^{-1}$ .

This discrepancy between theory and experiment, which was already observed with previous measurements, suggests that both our theory and PdV model may neglect a flux coupling heat and mass transport in unsaturated environment. As  $k_v k_B T / D \gg 1$  in our experiment, this additional flux suggested in our theory cannot explain this observation.

## CONCLUSION AND PERSPECTIVES

In this paper, we studied experimentally the evolution of water potential caused by a temperature gradient across a vapor in a closed system and obtain a value of  $-7.9 \pm 0.4 \text{ MPa} \cdot \text{K}^{-1}$  at  $21^\circ\text{C}$  in agreement with previous experimental results. We proposed a simple theory for this result, based on a physical description of the experimental situation. This theory is in agreement with PdV model for our experiment but suggests the existence of an additional flux coupling heat and water transport which may become relevant in nanoporous systems that can be encountered in geological or industrial context.

In the considered situation, both theories predict a variation of water potential of  $-8.47 \text{ MPa} \cdot \text{K}^{-1}$  at  $21^\circ\text{C}$ . Despite being close to the experimental value, a careful analysis of experimental uncertainties, mostly arising from the difficulty to control the imposed temperature difference, show that the discrepancy between theory and experiment is significant. This result leaves open the possibility of a missing element on our description of the coupled heat and mass transport in unsaturated porous media.

Future experiments with our system could provide quantitative measurements in realistic soils or in plants, in laboratory or in the field, in order to test PdV model more generally. The strong variation of water potential with temperature confirmed here highlights the necessity, well known by users of psychrometers, to ensure isothermal conditions or to apply a proper correction if it is not the case. This same caution applies to the use of our microtensiometer for the measurement of water potential in unsaturated media. Nonetheless, the design and mode of operation of the microtensiometer provides an important opportunity relative to thermocouple psychrometers: whereas the operation of psychrometers requires that the sensing element the thermocouple junction be exposed to vapor that, in turn, is exposed to the medium of interest, the nanoporous membrane of the microtensiometer can be put into direct contact with the medium of interest to favor thermal equilibrium and minimize the effect characterized here. Alternatively, for situations in which direct contact could lead to contamination, a conductive element, such as the copper strip used in this study (Fig. 3(b)), can help maintain thermal equilibrium with the sample. Work in our lab (unpublished) with the microtensiometer embedded in the xylem tissues of woody plants indicates that good thermal contact between the tissue and the device can indeed be achieved.

The authors thank Dr. Antoine Bérut, Prof. Bernard Castaing, Dr. Pierre Fleury, Dr. Michel Fruchart, Dr. Robin Guichardaz and Dr. David Lopes Cardozo for discussions on the theory, and Prof. John Albertson for discussions about the environmental context. The authors are grateful for Michael Santiago, Antoine Robin

and Siyu Zhu for the fabrication of the microtensiometers used in this study. The tensiometers were made in the Cornell Nanoscale Facility, an NNCI member supported by NSF grant ECCS-1542081. The authors acknowledge funding from AFOSR (FA9550-15-1-0052), NSF grant IIP 1500261, and Cornell College of Engineering.

*Declaration of Conflict of Interest* Co-author A.D.S. has a financial interest in FloraPulse Co., a company that holds a license to commercialize the microtensiometer used in this study.

---

\* Electronic address: pierre.lidon@u-bordeaux.fr

† Electronic address: ads10@cornell.edu

- [1] E. Fereres and M. Soriano, *Journal of Experimental Botany* **58**, 147 (2007).
- [2] P. D'Odorico and A. Porporato, *Proceedings of the National Academy of Science* **101**, 8848 (2004).
- [3] S. Seneviratne, T. Corti, E. Davin, M. Hirschi, E. Jaeger, I. Lehner, B. Orlowsky, and A. Teuling, *Earth-Science Reviews* **99**, 125 (2010).
- [4] J. Philip and D. de Vries, *Transactions of American Geophysical Union* **38**, 222 (1957).
- [5] J. Philip, *Journal of Meteorology* **14**, 354 (1957).
- [6] D. de Vries, *Transactions of the American Geophysical Union* **39**, 909 (1958).
- [7] D. de Vries, *International Journal of Heat and Mass Transfer* **30**, 1343 (1987).
- [8] M. Hassanizadeh and W. Gray, *Advances in Water Resources* **2**, 131 (1979).
- [9] M. Hassanizadeh and W. Gray, *Advances in Water Resources* **2**, 191 (1979).
- [10] M. Hassanizadeh and W. Gray, *Advances in Water Resources* **3**, 25 (1980).
- [11] P. Milly, *Water Resources Research* **18**, 489 (1982).
- [12] R. Slatyer and S. Taylor, *Nature* **4741**, 922 (1960).
- [13] I. Nassar and R. Horton, *Soil Science Society of America Journal* **56**, 1350 (1992).
- [14] I. Nassar and R. Horton, *Transport in Porous Media* **27**, 17 (1997).
- [15] M. Gran, J. Carrera, S. Olivella, and M. Saaltink, *Hydrology and Earth System Science* **15**, 2077 (2011).
- [16] M. Parlange, A. Cahill, D. Nielsen, J. Hopmans, and O. Wendroth, *Soil and Tillage Research* **46**, 5 (1998).
- [17] Y. Zeng, Z. Su, L. Wan, and J. Wen, *Journal of Geophysical Research* **116**, D20107 (2011).
- [18] Y. Zeng, Z. Su, L. Wan, and J. Wen, *Water Resources Research* **47**, W10529 (2011).
- [19] C. Rose, *Australian Journal of Soil Research* **6**, 31 (1968).
- [20] F. Rockwell, N. Holbrook, and A. Stroock, *Plant Physiology* **164**, 1741 (2014).
- [21] J. Cary, *Soil Science Society of America Proceedings* **30**, 428 (1966).
- [22] R. Jackson, R. Reginato, B. Kimball, and F. Nakayama, *Soil Science Society of America Proceedings* **38**, 861 (1974).
- [23] B. Scanlon, *Water Resources Research* **30**, 721 (1994).
- [24] A. Cahill and M. Parlange, *Water Resources Research* **34**, 731 (1998).
- [25] T. Saravanapavan and G. Salvucci, *Advances in Water Resources* **23**, 493 (2000).
- [26] J. Grifoll, J. Gastó, and Y. Cohen, *Advances in Water Resources* **28**, 1254 (2005).
- [27] H. Saito, J. Simunek, and B. Mohanty, *Vadose Zone Journal* **5**, 784 (2006).
- [28] M. Bittelli, F. Ventura, G. Campbell, R. Snyder, F. Gallegati, and P. Pisa, *Journal of Hydrology* **362**, 191 (2008).
- [29] M. Sakai, N. Toride, and J. Simunek, *Soil Science Society of America Journal* **73**, 707 (2009).
- [30] M. Novak, *Agricultural and Forest Meteorology* **150**, 1358 (2010).
- [31] M. Sakai, S. Jones, and M. Tuller, *Water Resources Research* **47**, W02547 (2011).
- [32] M. Novak, *Water Resources Research* **52** (2016).
- [33] C. Gurr, T. Marshall, and J. Hutton, *Soil Science* **74**, 335 (1952).
- [34] D. Cassel, D. Nielsen, and J. Biggar, *Soil Science Society of America Proceedings* **33**, 493 (1969).
- [35] D. Westcot and P. Wierenga, *Soil Science Society of America Proceedings* **38**, 9 (1974).
- [36] A. Cass, G. Campbell, and T. Jones, *Soil Science Society of America Proceedings* **48**, 25 (1984).
- [37] L. Bach, *Soil Science Society of America Journal* **56**, 37 (1992).
- [38] J. Heitman, R. Horton, T. Ren, I. Nassar, and D. Davis, *Soil Science Society of America Journal* **72**, 1197 (2008).
- [39] T. Wang and L. Su, *Journal of Cold Regions Engineering* **24**, 77 (2010).
- [40] K. Smits, A. Cihan, T. Sakaki, and T. Illangasekare, *Water Resources Research* **47**, W05540 (2011).
- [41] J. Han and Z. Zhou, *The Scientific World Journal* **2013**, 181240280 (2013).
- [42] J. Han, Z. Zhou, Z. Fu, and J. Wang, *Journal of hydrodynamics* **26**, 734 (2014).
- [43] D. Davis, R. Horton, J. Heitman, and T. Ren, *Soil Science Society of America Journal* **78**, 125 (2014).
- [44] C. Rose, *Australian Journal of Soil Research* **6**, 35 (1968).
- [45] R. Jackson, *Special Publication of Soil Science Society of America Proceedings* **5**, 37 (1973).
- [46] R. Jackson, B. Kimball, R. Reginato, and F. Nakayama, *Soil Science Society of America Proceedings* **37**, 505 (1973).
- [47] N. Monji, K. Hamotani, and Y. Omoto, *Bulletin of the University of Osaka* **42**, 61 (1990).
- [48] B. Scanlon, *Water Resources Research* **30**, 709 (1994).
- [49] G. Boulet, I. Braud, and M. Vauclin, *Journal of Hydrology* **193**, 114 (1997).
- [50] T. Yamanaka, A. Takeda, and J. Shimada, *Hydrological Processes* **12**, 2193 (1998).
- [51] B. Scanlon, K. Keese, R. Reedy, J. Simunek, and B. Andraski, *Water Resources Research* **39**, 1179 (2003).
- [52] H. Thomas, P. Cleall, D. Dixon, and H. Mitchell, *Géotechnique* **59**, 401 (2009).
- [53] L. Xiang, Z. Yu, L. Chen, J. Mon, and H. Lü, *Journal of Hydrologic Engineering* **17**, 565 (2012).
- [54] J. Vanderborght, T. Fetzer, K. Mosthaf, K. Smits, and R. Helmig, *Water Resources Research* **53**, WR019982 (2017).
- [55] H. Loescher, J. Jacobs, O. Wendroth, D. Robinson, G. Poulos, K. McGuire, P. Reed, B. Mohanty, J. Shanley, and W. Krajewski, *Bulletin of the American Meteorological Society* pp. 669–676 (2007).
- [56] M. Dixon and M. Tyree, *Plant, Cell and Environment* **7**, 693 (1984).

- [57] V. Pagay, M. Santiago, D. Sessoms, H. Huber, O. Vincent, A. Pharkya, T. Corso, A. Lakso, and A. Stroock, Lab on a chip **14**, 2806 (2014).
- [58] S. Wullschleger, M. Dixon, and D. Oosterhuis, Plant, Cell and Environment **11**, 199 (1988).
- [59] C. Soret, Comptes Rendus de l'Académie des Sciences de Paris **91**, 289 (1880).
- [60] M. Rahman and M. Saghir, International Journal of Heat and Mass Transfer **73**, 693 (2014).
- [61] S. Chapman and T. Cowling, *The Mathematical Theory of Non-Uniform Gases* (Cambridge University Press, 1990).
- [62] W. Köhler and K. Morozov, Journal of Non-Equilibrium Thermodynamics **41**, 151 (2016).
- [63] W. Haynes, *Handbook of Chemistry and Physics* (CRC, 2015).
- [64] B. Ghanbarian, A. Hunt, R. Ewing, and M. Sahimi, Soil Science Society of America Journal **77**, 1461 (2013).
- [65] O. Vincent, A. Szenicer, and A. Stroock, Soft Matter **12**, 6656 (2016).